THE JOURNAL OF PHYSICAL CHEMISTRY B
A JOURNAL OF THE AMERICAN CHEMICAL SOCIETY

pubs.acs.org/JPCB
Article

How Rigid Are Anthranilamide Molecular Electrets?

Omar O'Mari,[#] Moon Young Yang,[#] William Goddard,[*] and Valentine I. Vullev[*]

Cite This: J. Phys. Chem. B 2025, 129, 1750−1759
Read Online

ACCESS | Metrics & More | Article Recommendations | Supporting Information

ABSTRACT: As important as molecular electrets are for electronic materials and devices, conformational fluctuations strongly impact their macrodipoles and intrinsic properties. Herein, we employ molecular dynamics (MD) simulations with the polarizable charge equilibrium (PQEq) method to investigate the persistence length (L_P) of molecular electrets composed of anthranilamide (Aa) residues. The PQEq-MD dissipates the accepted static notions about Aa macromolecules, and L_P represents the shortest Aa rigid segments. The classical model with a single L_P value does not describe these oligomers. Introducing multiple L_P values for the same macromolecule follows the observed trends and discerns the enhanced rigidity in their middle sections from the reduced stiffness at their terminal regions. Furthermore, L_P distinctly depends on solvent polarity. The Aa oligomers maintain extended conformations in nonpolar solvents with L_P exceeding 4 nm, while in polar media, increased conformational fluctuations reduce L_P to about 2 nm. These characteristics set key guidelines about the utility of Aa conjugates for charge-transfer systems within organic electronics and energy engineering.

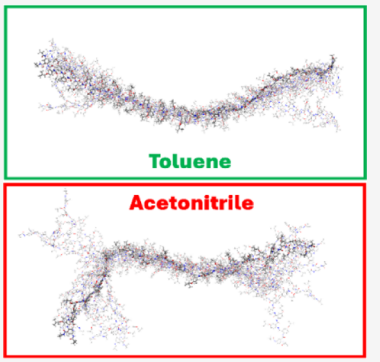

INTRODUCTION

In addition to their crucial importance for the mechanical integrity of a wide variety of materials and biomaterials, polymers and oligomers can mediate long-range transfer and transport of excitons and charges, such as electrons, holes and protons.[1−4] Hopping along the aromatic bases of double-stranded polynucleotides allows long-range hole transfer with pronounced high efficiency.[5−7] Protein and polypeptide helices mediate electron and hole tunneling at distances limited to a few nanometers.[8−12] Furthermore, these protein helical conformers possess enormous macrodipoles that can rectify the directionality of charge transfer (CT) and aid transmembrane ion transport.[12−18] Bioinspired molecular electrets composed of anthranilamide (Aa) residues, on the other side, have not only substantial macrodipoles, but also aromatic moieties along their backbones that can provide hopping sites for long-range electron and hole transfer.[19−24]

Electric dipoles are ubiquitous, and they strongly affect CT and the performance of electronic devices. With ordered electric dipole moments, electrets are electrostatic analogues of magnets, making them important components for device design and engineering. Polypeptide helices and Aa oligomers represent electrets where the dipoles are oriented in linear head-to-tail sequences. Layers of molecules with their dipoles aligned in a parallel manner represent another electret architecture. Dipoles of organic molecules, layered at the interfaces of electrical junctions, control the device performance.[25] Similarly, in field-effect transistors (FETs), electrets modulate threshold voltage, enabling the design of low-power devices with long-term stability.[26] Coating inorganic quantum dots with organic dipolar layers presents a strategy for improving the efficiency of photovoltaic cells.[27,28] In piezoelectric devices, dipoles enhance charge separation under mechanical stress, improving energy conversion efficiency.[29−31]

The conformational dynamics of polymers profoundly affect the efficiency of charge and energy transfer that they mediate. Dihedral rotations and bending of the backbone impact the extent of π-conjugation, the electronic coupling, and the orientation of transition dipole moments. Such conformationally driven transitions between adiabatic (strong coupling) and diabatic (weak coupling) regimes strongly affects charge mobility for transport via incoherent hopping.[7,32,33] The structural dynamics has also profound effects on long-range coherent charge transduction, i.e., occurring via superexchange tunneling mechanism.[34] Conformational fluctuations can induce shifting between constructive and destructive interference among parallel electronic-coupling pathways that lead to variations between efficient long-range CT and a complete shutdown of charge transduction.[35]

Electrostatic interactions play an enormous role in charge transfer, CT, and charge transport (CTr). In the equation for estimating CT thermodynamic driving forces, the Coulomb and Born-solvation terms account for electrostatic interaction, respectively, between the CT species, and between the CT species and the solvating media.[36,37] The theoretical treatment

Received: June 20, 2024
Revised: November 13, 2024
Accepted: November 14, 2024
Published: November 20, 2024

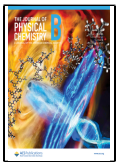

https://doi.org/10.1021/acs.jpcb.4c04103
J. Phys. Chem. B 2025, 129, 1750−1759

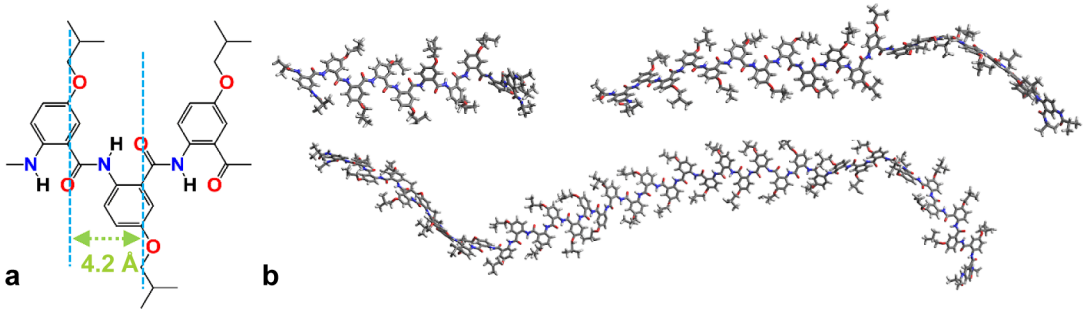

Figure 1. Structure of Aa oligomers comprising Box residues. (a) Chemical structure of Box trimer showing the repeating unit spanning 4.2 Å. (b) Conformations from MD for Aaa-Box$_{n-2}$-Aaa oligomers (n = 10, 20, and 40) in Tol, illustrating the flexibility of the macromolecules.

of polarons, which aid charge transduction through solids, has evolved since the 1930s to reach its current level of sophistication.[33] The electrostatic effects on CT and CTr are especially pronounced in low-dielectric constant media, such as organic materials. Coulombic charge trapping at electron-donor−acceptor interfaces is a serious source of losses for organic photovoltaics.[38] Extended charge delocalization provides a means for escaping such Coulomb traps,[29,30,39] warranting improved control over the effects of conformational dynamics on the extent of π-conjugation.

The molecular dynamics also affect bulk properties of materials, such as their dielectric constants, ε. Transition from liquid to solid phases lowers ε because of the loss in the orientational polarization, i.e., the loss of the ability of dipoles to orient along the external field.[40] Improving the flexibility of dipolar groups in solid materials allows for enhancing ε.[41] While high ε is beneficial for energy storage, i.e., high-capacity capacitors, and for preventing Coulomb trapping, the beneficial effects of molecular electrets on CT emerge with lowering medium polarity.[15,42,43] Furthermore, while electrets can mediate long-range CT and CTr, they must be insulators. Populating electrets with free changes counters their permanent dipoles, which removes the localized electric fields that make such systems electrets. In this respect, CT electrets resemble biological materials, such as DNA and proteins with sequences of electronically coupled redox centers, that can mediate long-range charge transduction.[6,44−46]

The importance of conformational dynamics for electronic properties of macromolecules and materials cannot be overstated. Persistence length (L_P) characterizes the conformational flexibility of polymers, which can be modeled as chains of rigid links hinged with flexible joints or as worm-like structures.[47,48] In this respect, L_P represents the longest stretch of the polymer chain that does not exhibit flexibility.[48−50]

According to broadly accepted notions, the Aa conjugates assume extended conformation supported by hydrogen bonds between the amides (Figure 1).[51] The structural information about these macromolecules, however, originates from work on short oligomers, i.e., dimers and trimers.[21,22,51] Employing molecular dynamics (MD) including polarization and charge rearrangement, implemented using the polarizable charge equilibrium (PQEq) method, allows expanding such studies to Aa structures with lengths exceeding 10 residues.[52−55] Our previous work shows that the macrodipoles of oligomers increase linearly with the oligomer length, strongly affected by solvent polarity and hydrogen-bonding interactions, and exceeding 100 D for conjugates composed of 20 and 40 residues.[52] Considering that organic molecules with dipoles smaller than 5 D can strongly affect the performance of devices,[25,27] the large dipoles of the Aa molecular electrets make them promising candidates for energy and electronic applications. These studies also reveal for the first time enormous fluctuations of the electret dipoles that emerge from solvent dynamics.[52] The dipole of an Aa 40-mer in dichloromethane and acetonitrile, for example, exhibits picosecond variations ranging between about 50 and 600 D.[52] It opens new paradigms of thinking about solvation effects on picosecond processes, such as fast CT.[56]

While the medium dynamics around the solvation cavity drives these dipole fluctuations, they do not occur independently from the variations of the Aa molecular electrets. It warrants improved understanding of the flexibility of the Aa oligomers that persistence length quantifies in a straightforward manner.

Herein, we employ PQEq-MD simulations to study conformational dynamics of Aa macromolecules and characterize their flexibility. Analysis of the MD results reveals that the L_P of Aa polymers can reach 10 residues, especially for nonpolar media. At the terminal regions, however, L_P decreases substantially. An increase in solvent polarity enhances the conformational fluctuations resulting in reduced L_P values.

RESULTS

MD Simulations. As a typical Aa macromolecule, we focus on conjugates composed of Box residues containing *iso*-butyl ether groups in the side chain (Figure 1a), at which the ether substituents lead to reversible electrochemical oxidation at large positive potentials making them feasible to use for transducing high-energy holes.[57] In comparison, an Aa residue with an *N*-amide at this position (denoted as Aaa) caps both ends of the oligomers due to its covalent connectivity with favorable electronic coupling for hole injection by photoexcited electron acceptors (Figure S1).[42,58]

For Aa oligomers with the Aaa-Box$_{n-2}$-Aaa structure (Figure S1), we examine three conjugates with different lengths (n = 10, 20, and 40) and investigate their dynamic behavior (Figure 1b). Our method allows explicit implementation of solvents with varying polarities: toluene (Tol; weak), dichloromethane (DCM; moderate), and acetonitrile (MeCN; strong). These solvents do not form hydrogen bonds with the backbone amides of the Aa oligomers, which is critical for maintaining structural rigidity.

In this study, we employ PQEq polarization and charge rearrangement, along with universal nonbonding (UNB) and universal hydrogen bonding (UHB) force fields, to accurately describe nonbonding interactions,[55,59,60] while using a modified universal force field (UFF) for the bonded interactions.[60] Successfully reproducing the dipoles of small aliphatic amides,

https://doi.org/10.1021/acs.jpcb.4c04103
J. Phys. Chem. B 2025, 129, 1750−1759

which were previously obtained experimentally from impedance spectroscopy and theoretically from quantum mechanics (QM) calculations,[40] provides validation of this methodology.[52] Our previous study reveals that the dynamic behavior of the macrodipoles manifests a clear dependency on both solvent polarity and polymer length and demonstrates an almost linear relationship between the average length of the oligomers, defined as the end-to-end distance, and the number of residues.[52] These oligomers, however, exhibit significant conformational fluctuations in the presence even of non-hydrogen-bonding solvents, as the MD simulations show (Figures 1b and 3d–l). This observation suggests that our understanding of dynamic behavior warrants further elucidation.

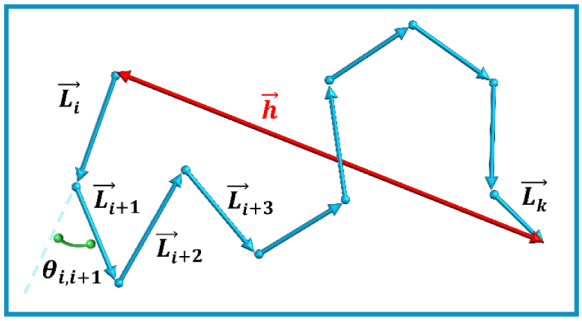

Figure 2. Depiction of a segment of a macromolecule (between the i^{th} and the k^{th} residue) as a flexible system with a contour length of $\sum_{j=i}^{k} L_j$. The angle $\theta_{i,j}$ depicts the direction that a vector $\vec{L}_j$ makes with a reference vector $\vec{L}_i$. The vector, connecting the head of $\vec{L}_i$ and the tail of $\vec{L}_j$, represents the end-to-end distance when $i = 1$, i.e., the first residue of the polymer, and $k = n$, i.e., the last residue of a polymer composed of n units. The length of each vector, $\vec{L}_j$, is the same, designated with L_B. The differences between the lengths of the shown arrows originate from the projection of the three-dimensional arrangement of these vectors in the plane of their two-dimensional representation of the figure.

Modeling Polymer Chains. Understanding the behavior of polymers through models is crucial for grasping their mechanical and thermodynamic properties. Assuming no interactions between the monomers, the *"ideal" models* of polymer chains describe such macromolecules well with the smallest number of parameters. Among them, the *freely jointed chain* (FJC) model is the simplest one. It represents polymers as linear chains of rigid segments connected with flexible bonds. The bond and torsion angles between the segments can assume any value with equal probability. Developed by Werner Kuhn in the FJC treatment, the *Kuhn length* (β_K) is the length of the rigid segments, also referred to as *Kuhn segments*.[61]

The FJC model provides a basic understanding of polymer flexibility but ignores the bond-angle and torsional constraints in macromolecules. In contrast, the *freely rotating chain* (FRC) model accounts for the structural features of chemical bonding and allows equiprobable torsional degrees of freedom while keeping the bond angles fixed. It incorporates a level of structural realism by accounting for the fixed spatial orientation between neighboring monomers. Taking this concept further, the *hindered rotation* (HR) model considers the potential energies along the rotational trajectories and employs the Boltzmann factor for estimating the probability for each torsion angle. Unlike the other models, the *worm-like chain* (WLC) model assumes continuous flexibility. That is, the flexibility along the polymer chain is not only between the rigid segments. In the WLC model, the persistence length, L_P, represents the longest stretch of a polymer chain behaving like a rigid rod. Therefore, L_P offers quantification of the bending stiffness of polymer chains.

The two critical lengths emerging from these conceptual models of polymers are L_P and β_K. Specifically, L_P is distance over which the direction of the polymer chain remains correlated, serving as a measure of the polymer stiffness.[62] Conversely, β_K represents the effective segment length while accounting for the local stiffness in an equivalent FJC treatment that approximates the behavior of a real polymer chain.[63] That is, β_K is a key characteristic emerging from an idealized model of a real polymer chain, which simplifies analysis while retaining the critical representation of the macromolecular mechanical properties.[48] The relationship between L_P and β_K is fundamental to understanding polymer dynamics and structure. The L_P characterizes the local stiffness of the chain, while the β_K scales the chain into an ideal model, facilitating the theoretical analysis of polymer properties. These lengths are pivotal in providing a bridge between microscopic interactions and macroscopic properties, such as the overall dimensions of polymer chains and their response to external forces.

These two lengths are correlated: a larger β_K results in a larger L_P, making the polymer stiffer. Conversely, a smaller β_K warrants enhanced flexibility of the polymer.

Estimating Persistence Length. The modeling involves partitioning the macromolecule into n arbitrary rigid segments, each with the same length L_B that is smaller than L_P (Figure 2). If the monomer units are rigid, they present a good choice for such arbitrary segments. The angle between any two rigid segments i and j is $\theta_{i,j}$ (Figure 2). The mean of the squared end-to-end distance (h, Figure 2) provides estimates for the β_K that, for WLC, is usually about twice larger than L_P:[48,49,62,64,65]

$$\langle h^2 \rangle \approx \beta_K n L_B \approx 2 L_P n L_B \tag{1}$$

The structures from the MD simulations provide straightforward estimates for h, of the Aa oligomers. Averaging the squares of h for all frames from a simulation run yields $\langle h^2 \rangle$ needed for calculating β_K and L_P (eq 1). The span of the repeating residue unit in the extended conformations of the oligomers defines the magnitude L_B of the link vectors, i.e., $L_B = 4.2$ Å (Figure 1a). The values of β_K and L_P, obtained for the Aa conjugates using eq 1, manifest dependence on the length of the oligomers and the solvent (Figure 3c, Table S7). The L_P of macromolecules depends not only on their intrinsic properties but also on the surrounding environment, as the model from Odijk, Skolnick, and Fixman describes for charged polymers, for example.[66,67] Nevertheless, the oligomer length should not affect L_P. This discrepancy warrants resorting to an improved analysis for obtaining L_P.

The statistics of h characterizes the dimensions of a macromolecule:

$$\langle h^2 \rangle = \left\langle \left(\sum_{i=1}^{n} \vec{L}_i \right) \cdot \left(\sum_{j=1}^{n} \vec{L}_j \right) \right\rangle \tag{2a}$$

The expanded terms result in self-correlation when $i = j$ and the interbond correlations when $i \neq j$:

https://doi.org/10.1021/acs.jpcb.4c04103
J. Phys. Chem. B 2025, 129, 1750−1759

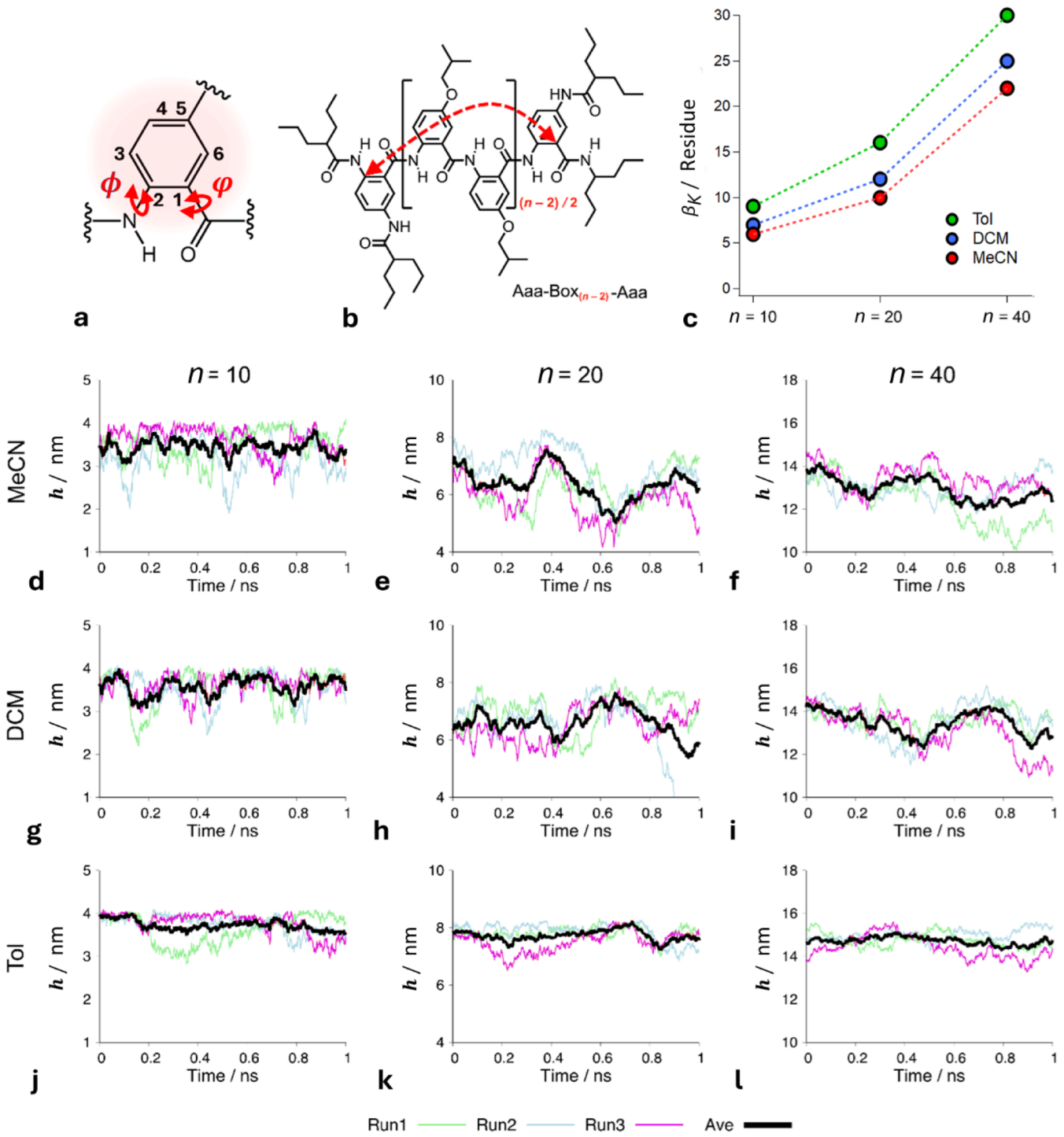

Figure 3. Visualization of the variability of the end-to-end distance, h, of Aa oligomers with 10 to 40 residues across different solvent environments. (a) A single residue of Aa indicating the numbering of the carbon atoms and attachments of the *N*- and *C*-terminal amides. The dihedral angles, ϕ and φ, quantify the rotation around the bonds between the amides and the aromatic ring responsible for the conformational variations along the backbones of the electret oligomers. (b) Chemical structure illustrating the end-to-end span, h, across the oligomer. (c) The Kuhn length, β_K, of oligomers with number of residues, n = 10, 20 and 40, in different solvent environments, i.e., Tol, DCM, and MeCN. (d-l) Variation of h and its averages through the 1 ns MD simulations for the three trials of the oligomers with (d,g,j) 10, (e,h,k) 20 and (f,i,l) 40 residues (d-f) in MeCN, (g-i) in DCM and (j-l) in Tol.

https://doi.org/10.1021/acs.jpcb.4c04103
J. Phys. Chem. B 2025, 129, 1750−1759

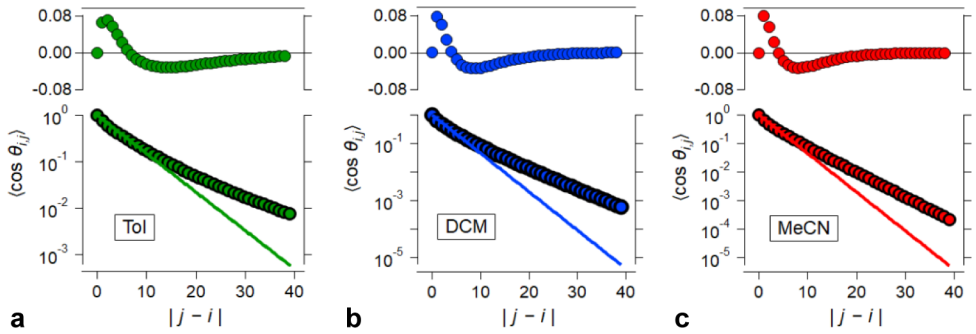

Figure 4. Correlation decays, i.e., $\langle \cos\theta_{i,j} \rangle$ vs |j−i| (the circular markers), derived from the 1 ns MD simulations of the Aa oligomers (Figure 3d-l), along with monoexponentially data fits (eq 3a) (solid lines). The data-fit residuals are displayed on the top of each graph. Decays of $\langle \cos\theta_{i,j} \rangle$ for: (a) Tol, the data fit yields L_P = 5.3 residues; (b) DCM, the data fit yields L_P = 3.2 residues; and (c) MeCN, the data fit yields L_P = 3.2 residues.

$$\langle h^2 \rangle = \sum_{i=1}^{n} \vec{L_j} \left(\sum_{j=1}^{i-1} \langle \vec{L_i} . \vec{L_j} \rangle + \langle \vec{L_i}^2 \rangle \sum_{j=i+1}^{n} \langle \vec{L_i} . \vec{L_j} \rangle \right)$$

$$= \sum_{i=1}^{n} \langle \vec{L_i}^2 \rangle + L_B^2 \sum_{i=1}^{n} \left(\sum_{j=1}^{i-1} (\cos\theta_{i,j})^{i-j} + \sum_{j=i+1}^{n} (\cos\theta_{i,j})^{j-i} \right)$$

$$= nL_B^2 + L_B^2 \sum_{i=1}^{n} \left(\sum_{k=1}^{i-1} \cos^k \theta_{i,j} + \sum_{k=1}^{n-i} \cos^k \theta_{i,j} \right) \tag{2b}$$

$$\sum_{i=1}^{n} \left(\sum_{k=1}^{i-1} \cos^k \theta_{i,j} + \sum_{k=1}^{n-i} \cos^k \theta_{i,j} \right) \cong$$

$$2 \sum_{i=1}^{n} \sum_{k=1}^{\infty} \cos^k \theta_{i,j} = 2n \sum_{k=1}^{\infty} \cos^k \theta_{i,j} = 2n \frac{\cos \theta_{i,j}}{1 - \cos \theta_{i,j}} \tag{2c}$$

Thus,

$$\langle h^2 \rangle = nL_B^2 + 2nL_B^2 \frac{\cos \theta_{i,j}}{1 - \cos \theta_{i,j}} = nL_B^2 \frac{1 + \cos \theta_{i,j}}{1 - \cos \theta_{i,j}} \tag{2d}$$

One key aspect of this analysis involves measuring the alignment between different rigid segments (not necessarily next to each other) of the polymer backbone, which is quantified using the cosine of the angle between them, $\cos\theta_{i,j}$ (Figure 2). This angle $\theta_{i,j}$ measures how well two segments, *i* and *j*, align with each other. Thus, $\cos\theta_{i,j}$ = 1 represents perfect alignment and $\cos\theta_{i,j}$ = 0 indicates no correlation between the orientations of the two segments. As the distance between the arbitrary rigid segments,|*j*-*i*|, increases along the polymer chain, the alignment typically decreases, a phenomenon known as a decay of $\cos\theta_{i,j}$, representing a loss of orientational correlation. The rate of this decay is a critical indicator of the polymer flexibility. In a stiff polymer, segments remain aligned over relatively long distances and $\cos\theta_{i,j}$ decays slowly as the separation between segments increases. In a flexible polymer, on the other hand, the alignment decays at a short distance, indicating enhanced flexibility of the backbone. An exponential function with L_P as the inverse of the decay constant can describe this loss of correlation:[48,63,68]

$$\langle \cos \theta_{i,j} \rangle = \exp\left\{ -\frac{|j - i| L_B}{L_P} \right\} \tag{3a}$$

Hence, the persistence length can be expressed in terms of the averaged correlation between the i^{th} and j^{th} vectors:

$$L_P = -|j - i| L_B \ln^{-1}(\langle \cos \theta_{i,j} \rangle) \tag{3b}$$

The significance of this decay and its relationship to the L_P and β_K extends beyond structural considerations. In molecular electrets like Aa oligomers, conformational flexibility has a direct impact on their electronic properties, such as their macrodipoles, the electronic-coupling pathways they provide for charge transfer, and the exciton mobility they mediate. Bending of the backbone that breaks the electronic coupling, for example, hinders charge transfer and charge transport. Variations of polymer macrodipoles originating from their flexibility can induce additional effects on the charge-transduction dynamics. These multifaceted effects originating from backbone structural fluctuations make L_P a critical parameter for predicting the performance of such materials in electronic and energy applications.

The MD simulations reveal that dihedral rotations around the bonds between the amides and the aromatic rings are principally responsible for the conformational variations along the backbones of the electret oligomers (Figure 3a). The aromatic rings of the Aa residues, on the other hand, are relatively rigid with the positions of their atoms showing negligibly small fluctuations relative to one another. This feature makes them a perfect choice for defining the orientation of the link vectors $\vec{L_i}$ to $\vec{L_j}$ for the model (Figure 2). For each residue, points from carbon 2, bearing its *N*-terminal amide, to the carbon at position 1 connected to the carbonyl carbon of its *C*-terminal amide (Figure 3a). The relative correlation to the orientation of any pair of $\vec{L_i}$ to $\vec{L_j}$, corresponding to the i^{th} and j^{th} residues, along the Aa oligomer chain produces $\theta_{i,j}$. By definition, $\langle \cos\theta_{i,j} \rangle$ is the average of the cosine values of $\theta_{i,j}$ and obtained from the multiple frames along the trajectories produced by the MD simulations. This average of the correlation angles formulates the behavior of $\theta_{i,j}$. Exponential fits of these correlations vs the residue position *j* in relevance to residue *i* (eq 3a) produce L_P.

What Do the Results for Aa Conjugates Mean?

Sampling the $\cos\theta_{i,j}$ decays in various directions reveals that the "traditional" exponential model of L_P (eq 3a) does not accurately represent the conformational behavior of the Aa macromolecules. The residual from the monoexponentially fits exhibit patterns with amplitudes that amount to about 10% of the $\langle \cos\theta_{i,j} \rangle$ values (Figure 4). Durbin−Watson (DW) statistics allow testing of how well a selected fitting model describes the analyzed results. Specifically, DW quantifies autocorrelation patterns in the residuals that the data fits do not depict.[69−72] Low DW values, such as DW $\lesssim$ 1.2, indicate positive

https://doi.org/10.1021/acs.jpcb.4c04103
J. Phys. Chem. B 2025, 129, 1750−1759

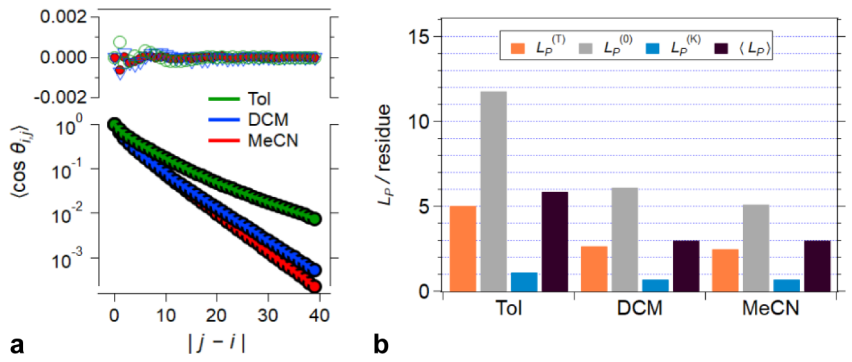

Figure 5. $\langle \cos\theta_{i,j} \rangle$ correlation decays and the L_P of Aa oligomers for solvents with different polarity. (a) Representative correlation decays for Tol, DCM and MeCN, along with the triexponential fits (eq 4) and the corresponding residuals from these SCF analysis. The $\theta_{i,j}$ values are extracted from the MD simulation for the electret surrounded by explicitly introduced Tol, DCM and MeCN solvents, and the corresponding cos $\theta_{i,j}$ are averaged of all the segmented frames from the 1 ns MD simulations. (b) The L_P of the Aa electrets obtained from the triexponential SCF fits and assigned to $L_P^{(0)}$, $L_P^{(T)}$ and $L_P^{(K)}$, based on the patterns from the GF analysis (see Supporting Information), for the Aa oligomers with n = 10, 20, and 40 residues. The amplitude averages of the L_P from the triexponential fits, $\langle L_P \rangle = \frac{\sum_{i=1}^{n} A_i \times L_{P_i}}{\sum_{i=1}^{n} A_i}$ provides a single value for the L_P considering the contributions from all the components.

autocorrelation, i.e., the fits yield systematic patterns questioning the validity of the regression model. The analysis of the monoexponentially data fits for the Aa oligomers produces DW varying between 0.2 and 0.5 across the different solvents, which is consistent with the observed patterns in the residuals (Figure 4) and warrants improving the model for describing the distance dependence of the loss of the $\langle \cos\theta_{i,j} \rangle$ correlations.

Increasing the number of exponential terms of fit functions offers a means to account for the correlation patterns in the observed residuals, which sets the motivation for modifying eq 3a:

$$\langle \cos\theta_{i,j} \rangle = \sum_{k=1}^{N} A_k \exp\left\{ -\frac{|j-i| L_B}{L_{P_k}} \right\} \quad (4)$$

Three exponential terms provide good fits for the different correlation decays. They yield DW of about 1.8 for all three solvents indicating minimal autocorrelation between residuals, (Table S9) allowing confident evaluation of the data sets using eq 2c. Considering that the maximum value that $\langle \cos\theta_{i,j} \rangle$ can assume is one indicating a complete correlation, the sum of the amplitudes in eq 4 is always unity.

For each solvent, three sets of L_P values emerge from the single-curve-fit (SCF) multiexponential analysis of the decrease in $\langle \cos\theta_{i,j} \rangle$ along different i-to-j spans. For the different Aa oligomers in Tol, for example, such multiexponential analysis produces L_P values of about: (1) L_{P1} = 4.9 nm, corresponding to approximately 12 Aa residues, (2) L_{P2} = 2.1 nm, corresponding to 5 residues, and (3) L_{P3} = 0.5 nm, corresponding to a single Aa residue.

The corresponding amplitudes for the L_{P1}, L_{P2} and L_{P3} terms are A_1 = 0.3, A_2 = 0.43 and A_3 = 0.26. For DCM and MeCN, the triexponential SCF analyses produce similar patterns with three L_P values. An increase in solvent polarity reduces the amplitude of the term with the longest L_P (Table S9).

To elucidate what these three different L_P represent, we resort to a global-fit (GF) analysis of correlation decays, where $\theta_{i,j}$ spans over different segments of the oligomers (Figure S2, Table S8). Holding each of the L_P, i.e., L_{P1}, L_{P2} and L_{P3} (eq 4), the same for all correlation decays, the GF allows the amplitudes A_1, A_2 and A_3 to vary freely among the different sets of $\langle \cos\theta_{i,j} \rangle$ vs $|j-i|$.

For Tol, the three L_P values that the GF produces are 3.8 nm, corresponding to 9 residues; 1.7 nm, corresponding to 4 residues and 0.5 nm corresponding to one residue. For the $\theta_{i,j}$ segments that span over the middle sections of the oligomers and exclude the terminal regions, this GF analysis (for Tol) yields the largest amplitude of 0.76 for L_P = 3.8 nm, i.e., 9 residues. Shifting the $\theta_{i,j}$ spans toward the termini, increases the amplitude for L_P = 1.7 nm, i.e., 4 residues, to 0.74, while decreasing the contributions from the L_P = 9 residue to amplitude of 0.06 (Table S8). The GF yields a third component of L_P of 0.5 nm, corresponding to a single residue, with amplitudes of around 0.2 persisting in all different segments for Tol (Table S8).

These results allow ascribing the largest L_P value for each solvent to the intrinsic L_P of an Aa polymer, $L_P^{(0)}$, without the effects of conformational fluctuations at its termini. The term with the intermediate L_P dominates each triexponential data fit of the segment at the terminal regions of the oligomers (Table S8). Therefore, these intermediate L_P values represent the $L_P^{(T)}$ emerging at the termini of the Aa conjugates.

For all solvents, the shortest L_P that the triexponential GF analysis yields amount to about one residue. These small L_P values represent the emergence of kinks along the Aa oligomers where both backbone amides of the same residue twist considerably out of the plane of its aromatic ring. This consideration allows designating the shortest length as $L_P^{(K)}$ with an amplitude that contributes about 5% to 20% to the correlation decays at the different regions of the oligomers (Table S8).

These ascriptions of the results from the GF analysis offer the basis for designating the different L_P that the SCF fits yield. For each triexponential SCF fit, the largest L_P value most likely designates $L_P^{(0)}$, the intermediate L_P value – $L_P^{(T)}$; and the smallest L_P value – $L_P^{(K)}$ (Figure 5). For each solvent, shifting from the middle of the oligomers to their terminal regions, decreases the L_P by a factor of 2, i.e., $L_P^{(T)} \approx 0.5 L_P^{(0)}$ (Table S9). This trend is consistent with conformational destabilization at termini of macromolecules, especially when hydrogen bonding and steric interactions restrict the structural fluctuations along the polymer chain.[73−75]

Conversely, increasing solvent polarity reduces the three L_P components representing the stiffness of the Aa oligomers (Figure 5b). In addition, the trends from the fits of the $\langle \cos\theta_{i,j} \rangle$

https://doi.org/10.1021/acs.jpcb.4c04103
J. Phys. Chem. B 2025, 129, 1750−1759

decays spanning from the first to the last residue of the electrets show that an increase in solvent polarity increases the amplitude for the $L_P^{(T)}$ terms, while decreasing that for $L_P^{(0)}$ (Figure 5b, Table S9). Previous studies on Aa conjugates show that increased solvent polarity destabilizes the π-conjugation between the aromatic rings and the amides, and reduces their hydrogen-bonding capabilities.[52] These polarity-induced changes weaken the constraints for dihedral fluctuations, which is consistent with the observed decrease in all L_P values upon transitioning from Tol to DCM and MeCN. That is, nonpolar solvents favor planarity, which enhances the stiffness characteristics of the Aa backbone, such as h, β_K and $L_P^{(0)}$. It is important to emphasize that lowering medium polarity increases not only L_P of the Aa electrets, but also the effects of their dipoles on CT,[42,43] making these conjugates immensely attractive for applications in low-dielectric-constant environments.

DISCUSSION

As commonly defined (eq 3a), L_P often fails to capture the local intrinsic flexibility, especially in terminal regions. Due to the reduced number of nearest-neighbor interactions, the flexibility at the termini increases and L_P markedly decreases. This trend is particularly evident and extensively studied in biopolymers, such as polypeptide helices.

Electrostatic interactions and hydrogen bonding play a key role for stabilizing the terminal regions of polypeptide α-helices.[76,77] For stabilizing the secondary conformation, early work focuses on the Coulombic interactions between the helix macrodipoles and the terminal charges.[78] The high dielectric constant of the usually used solvating media, however, diminishes the dipole effects.[79,80] Therefore, the interactions between charged and dipolar groups localized at the termini emerge to have a dominating contributions to the helix stability.[76,80]

As important as the electrostatics are, they function in synergy with other interactions. Chemical modifications for eliminating disruptive charges can also introduce sites for hydrogen bonding that stabilizes the helix folds at the termini.[81] Considering hydrogen bonding, along with hydrophobic interactions, has led to the emergence of sophisticated strategies for capping the terminal regions of polypeptides to stabilize their helical secondary conformation.[82]

The development of strategies for stabilizing biopolymer conformations have grown for many decades. In contrast, we are just beginning to unravel the structural features of Aa molecular electrets. The structural differences between the helical conformers and the extended Aa conjugates precludes direct translation of the current strategy for stabilizing the termini of the Aa oligomers. For example, electrostatic interactions that induce stretching forces along the principal axes, while causes disruptive unfolding of helices, can have the potential to stabilize the Aa extended conformation at the termini. Therefore, placing negative charges at the *N*-terminus and positive charges at the *C*-terminus of Aa oligomers can prove beneficial. The Coulombic interactions between such terminal charges and the Aa macrodipole (which points from the *N*- to the *C*-terminus) should induce forces favoring the extended conformation, especially in low-polarity media. In addition, such charges will enhance the dipole field. Exploration of this idea, along with strategies for hydrogen-bonding capping of the terminal amides of Aa electrets, is indeed beyond the scope of this study.

In organic electronics, the design of systems for mediating long-range CT hinges on the intrinsic properties of polymers and oligomers. Among these properties, L_P — a measure of molecular stiffness and the range over which the segments of polymers remain directionally correlated — emerges as a critical factor. Conformational flexibility and dynamics strongly affect electronic coupling and CT kinetics.[83]

A number of biological macromolecules assume helical conformations with extended shapes manifesting remarkable stiffness. Such rod-shaped structures reveal key paradigms for the design of molecular wires.[84−86] For example, double-stranded DNA (dsDNA) is renowned for its large L_P, typically between 40 to 60 nm, corresponding to approximately 120 to 180 base pairs.[87−89] The electrostatic repulsion between the negatively charged backbone phosphates stabilizes the extended conformation of DNA. Lowering the ionic strength of the solvating media decreases the electrostatic screening of the phosphate charges and, therefore, can drive dsDNA to assume L_P exceeding 100 nm, i.e., > 290 base pairs.[90] Conversely, protein-nucleic acids (PNAs) comprise noncharged backbones making them more flexible than their DNA analogues.[91] Hence, the L_P of double-stranded PNA (dsPNA) is about 35 nm, i.e., shorter than L_P of dsDNA.[92]

Considering this structural rigidity of polynucleotides, it is not a surprise that dsDNA and dsPNA can serve as molecular wires, effectively mediating hole transfer (HT) over tens of nanometers.[6,93] In addition to their relative rigidity, these macromolecules mediate hole hopping (with holes delocalized over several base pairs). Along dsDNA, HT rates show minimum distance dependence beyond the first 3 to 4 base pairs following the initial charge separation.[6]

Compared with dsDNA and dsPNA, protein and polypeptide helices exhibit significantly shorter L_P, generally ranging from about 2 to 20 nm.[94] When subjected to alkaline environment, poly-L-lysine (PLL) forms righthanded α-helices with L_P of 15 to 21 nm. Unlike α-helices, polyprolines do not have hydrogen-bonding network to support their secondary structure. Nevertheless, polyproline type II (PPII) helix is an extended conformer with L_P of about 3 to 4 nm.[95] While a report of PPII L_P exceeding 10 nm further confirms the rigidity of these helical polypeptides, the impressive results of L_P = 7 nm and L_P = 13 nm are from studies on oligomers containing, respectfully, only two and one proline residues.[96] Polypeptides of achiral non-native amino acids assuming 3_{10}-helical conformations with L_P that ranges from about 3 nm (for polar media) to 37 nm (for nonpolar media).[97] This behavior is comparable to the observed effect of medium polarity on the L_P of Aa oligomers (Figure 5b).

Unlike polynucleotides, polypeptides of α-amino acids mediate CT only via tunneling along their backbones. Injecting holes into the peptide bonds (which are aliphatic carboxyl amides) leads to oxidative degradation.[98] precluding hopping as a potential CT mechanism. These features limit the utility of polypeptide helices as effective mediators of effective CT to about 2 nm.[8,9,11] Therefore, the inherent $L_P \gtrsim 3$ nm for these macromolecular structures ensures that the conformational flexibility is not necessarily the limiting factor for their propensity to efficiently mediate CT. One important feature of helical polypeptides is their enormous macrodipole that can reach 5 D per residue,[12] making them attractive molecular electrets that can directionally rectify CT rates.[15,16,99,100]

This study shows that Aa conjugates manifest L_P comparable to those of polypeptide helices. These Aa oligomers exhibit $\langle L_P \rangle$, between 1.4 and 2.5 nm, while their $L_P^{(0)}$ (i.e., without the effects of the termini and the kinks) amount to about 2 and 5 nm (Figure 5b). Similar to helical polypeptides, Aa oligomers are

https://doi.org/10.1021/acs.jpcb.4c04103
J. Phys. Chem. B 2025, 129, 1750−1759

electrets and possess large macrodipoles that can rectify CT.[21,22,42,43,52]

Conversely, the aromatic moieties of the Aa oligomers provide sites for charge hopping along their backbones needed for long-range CT, similar to that of polynucleotides. This feature of the Aa electrets illustrates a principal advantage over their biological polypeptide counterparts. The cross section of Aa polymer chain is about 1 nm wide and 0.2 nm high. This structural feature makes the Aa conjugates quite thinner than dsDNA, which has circular cross section with a diameter of about 2 nm, and even than polypeptide α-helices that have a diameter of about 1 nm.

CONCLUSIONS

Based on the L_P analysis, anthranilamide oligomers with lengths that do not exceed five residues assume relatively rigid extended conformations. Nonpolar solvating media enhance this conformational rigidity placing these bioinspired macromolecules on par with a number of biological structures. The relatively large persistence length, the large macrodipoles, the thin cross sections and the ability to mediate long-range CT make anthranilamide molecular electrets uniquely promising for organic electronics and energy-conversion systems.

ASSOCIATED CONTENT

Supporting Information

The Supporting Information is available free of charge at https://pubs.acs.org/doi/10.1021/acs.jpcb.4c04103.

Theoretical and computational details including the choices of simulation parameters and references along with parameter fits and their associated L_P and amplitude values (PDF)

AUTHOR INFORMATION

Corresponding Authors

William Goddard − *Materials and Process Simulation Center, California Institute of Technology, Pasadena, California 91125, United States;* orcid.org/0000-0003-0097-5716; Email: wag@caltech.edu

Valentine I. Vullev − *Department of Bioengineering, University of California, Riverside, California 92521, United States; Department of Chemistry, Department of Biochemistry, and Materials Science and Engineering Program, University of California, Riverside, California 92521, United States;* orcid.org/0000-0002-3416-9686; Email: vullev@ucr.edu

Authors

Omar O'Mari − *Department of Bioengineering, University of California, Riverside, California 92521, United States;* orcid.org/0000-0002-4742-4623

Moon Young Yang − *Materials and Process Simulation Center, California Institute of Technology, Pasadena, California 91125, United States;* orcid.org/0000-0003-4436-8010

Complete contact information is available at: https://pubs.acs.org/10.1021/acs.jpcb.4c04103

Author Contributions

#O.O. and M.Y.Y. contributed equally.

Notes

The authors declare no competing financial interest.

ACKNOWLEDGMENTS

V.I.V. and O.O. thank the U.S. National Science Foundation (grant number CHE 2154609) and the American Chemical Society Petroleum Research Fund (grant number 60651-ND4) for supporting these studies. M.Y.Y. and W.A.G. were funded by the NSF (grant CBET 2311117, program manager Robert McCabe). M.Y.Y. and W.A.G. also used resources of the National Energy Research Scientific Computing Center, a DOE Office of Science User Facility supported by the Office of Science of the U.S. Department of Energy under Contract No. DE-AC02-05CH11231 using NERSC award BES-ERCAP0024109.

REFERENCES

(1) Wan, Q.; Thompson, B. C. Control of Properties through Hydrogen Bonding Interactions in Conjugated Polymers. *Adv. Sci.* **2024**, *11*, 2305356.

(2) Khasbaatar, A.; Xu, Z.; Lee, J.-H.; Campillo-Alvarado, G.; Hwang, C.; Onusaitis, B. N.; Diao, Y. From Solution to Thin Film: Molecular Assembly of π-Conjugated Systems and Impact on (Opto) electronic Properties. *Chem. Rev.* **2023**, *123*, 8395−8487.

(3) Ding, L.; Yu, Z.-D.; Wang, X.-Y.; Yao, Z.-F.; Lu, Y.; Yang, C.-Y.; Wang, J.-Y.; Pei, J. Polymer semiconductors: synthesis, processing, and applications. *Chem. Rev.* **2023**, *123*, 7421−7497.

(4) Fahlman, M.; Fabiano, S.; Gueskine, V.; Simon, D.; Berggren, M.; Crispin, X. Interfaces in organic electronics. *Nat. Rev. Mater.* **2019**, *4*, 627−650.

(5) Hart, S. M.; Gorman, J.; Bathe, M.; Schlau-Cohen, G. S. Engineering Exciton Dynamics with Synthetic DNA Scaffolds. *Acc. Chem. Res.* **2023**, *56*, 2051−2061.

(6) Venkatramani, R.; Keinan, S.; Balaeff, A.; Beratan, D. N. Nucleic acid charge transfer: Black, white and gray. *Coord. Chem. Rev.* **2011**, *255*, 635−648.

(7) Derr, J. B.; Tamayo, J.; Clark, J. A.; Morales, M.; Mayther, M. F.; Espinoza, E. M.; Rybicka-Jasińska, K.; Vullev, V. I. Multifaceted aspects of charge transfer. *Phys. Chem. Chem. Phys.* **2020**, *22*, 21583−21629.

(8) Gray, H. B.; Winkler, J. R. Electron transfer in proteins. *Annu. Rev. Biochem.* **1996**, *65*, 537−561.

(9) Vullev, V. I.; Jones, G. Photoinduced charge transfer in helical polypeptides. *Res. Chem. Intermed.* **2002**, *28*, 795−815.

(10) Beratan, D. N.; Onuchic, J. N.; Winkler, J. R.; Gray, H. B. Electron-Tunneling Pathways in Proteins. *Science* **1992**, *258*, 1740−1741.

(11) Gray, H. B.; Winkler, J. R. Long-range electron transfer. *Proc. Natl. Acad. Sci. U.S.A.* **2005**, *102*, 3534−3539.

(12) Shin, Y.-G. K.; Newton, M. D.; Isied, S. S. Distance dependence of electron transfer across peptides with different secondary structures: the role of peptide energetics and electronic coupling. *J. Am. Chem. Soc.* **2003**, *125*, 3722−3732.

(13) Hol, W. G. J. Effects of the α-helix dipole upon the functioning and structure of proteins and peptides. *Adv. Biophys.* **1985**, *19*, 133−165.

(14) Dutzler, R.; Campbell, E. B.; Cadene, M.; Chait, B. T.; MacKinnon, R. X-ray structure of a ClC chloride channel at 3.0 Å reveals the molecular basis of anion selectivity. *Nature* **2002**, *415*, 287−294.

(15) Galoppini, E.; Fox, M. A. Effect of the electric field generated by the helix dipole on photoinduced intramolecular electron transfer in dichromophoric α-helical peptides. *J. Am. Chem. Soc.* **1996**, *118*, 2299−2300.

(16) Yasutomi, S.; Morita, T.; Imanishi, Y.; Kimura, S. A molecular photodiode system that can switch photocurrent direction. *Science* **2004**, *304*, 1944−1947.

(17) Doyle, D. A.; Cabral, J. M.; Pfuetzner, R. A.; Kuo, A.; Gulbis, J. M.; Cohen, S. L.; Chait, B. T.; MacKinnon, R. The structure of the potassium channel: molecular basis of K+ conduction and selectivity. *Science* **1998**, *280*, 69−77.

(18) Derr, J. B.; Tamayo, J.; Espinoza, E. M.; Clark, J. A.; Vullev, V. I. Dipole-induced effects on charge transfer and charge transport. Why do molecular electrets matter? *Can. J. Chem.* **2018**, *96*, 843−858.
(19) Vullev, V. I. From biomimesis to bioinspiration: what's the benefit for solar energy conversion applications? *J. Phys. Chem. Lett.* **2011**, *2*, 503−508.
(20) Espinoza, E. M.; Larsen, J. M.; Vullev, V. I. What makes oxidized N-acylanthranilamides stable? *J. Phys. Chem. Lett.* **2016**, *7*, 758−764.
(21) Xia, B.; Bao, D.; Upadhyayula, S.; Jones, G.; Vullev, V. I. Anthranilamides as bioinspired molecular electrets: experimental evidence for a permanent ground-state electric dipole moment. *J. Org. Chem.* **2013**, *78*, 1994−2004.
(22) Ashraf, M.; Millare, B.; Gerasimenko, A. A.; Bao, D.; Pandey, R. R.; Lake, R. K.; Vullev, V. I. Theoretical design of bioinspired macromolecular electrets based on anthranilamide derivatives. *Biotechnol. Prog.* **2009**, *25*, 915−922.
(23) Rybicka-Jasinska, K.; Vullev, V. I. Molecular electrets - Why do dipoles matter for charge transfer and excited-state dynamics? *J. Photochem. Photobiol., A* **2020**, *401*, 112779.
(24) Larsen, J. M.; Espinoza, E. M.; Vullev, V. I. Bioinspired molecular electrets: bottom-up approach to energy materials and applications. *J. Photonics Energy* **2015**, *5*, 055598.
(25) Vilan, A.; Shanzer, A.; Cahen, D. Molecular control over Au/GaAs diodes. *Nature* **2000**, *404*, 166−168.
(26) Zhang, X.; Zhao, J.; Xie, P.; Wang, S. Biomedical applications of electrets: recent advance and future perspectives. *J. Funct. Biomater.* **2023**, *14*, 320.
(27) Shalom, M.; Ruhle, S.; Hod, I.; Yahav, S.; Zaban, A. Energy level alignment in CdS quantum dot sensitized solar cells using molecular dipoles. *J. Am. Chem. Soc.* **2009**, *131*, 9876−9877.
(28) Santra, P. K.; Palmstrom, A. F.; Tanskanen, J. T.; Yang, N.; Bent, S. F. Improving performance in colloidal quantum dot solar cells by tuning band alignment through surface dipole moments. *J. Phys. Chem. C* **2015**, *119*, 2996−3005.
(29) Balzer, D.; Kassal, I. Delocalisation enables efficient charge generation in organic photovoltaics, even with little to no energetic offset. *Chem. Sci.* **2024**, *15*, 4779−4789.
(30) Li, Q.; Wang, R.; Yu, T.; Wang, X.; Zhang, Z.-G.; Zhang, Y.; Xiao, M.; Zhang, C. Long-range charge separation enabled by intramoiety delocalized excitations in copolymer donors in organic photovoltaic blends. *J. Phys. Chem. Lett.* **2023**, *14*, 7498−7506.
(31) Ma, Y.; Gong, J.; Zeng, P.; Liu, M. Recent progress in interfacial dipole engineering for perovskite solar cells. *Nanomicro Lett.* **2023**, *15*, 173.
(32) Deng, W.-Q.; Goddard, W. A. Predictions of hole mobilities in oligoacene organic semiconductors from quantum mechanical calculations. *J. Phys. Chem. B* **2004**, *108*, 8614−8621.
(33) Franchini, C.; Reticcioli, M.; Setvin, M.; Diebold, U. Polarons in materials. *Nat. Rev. Mater.* **2021**, *6*, 560−586.
(34) Prytkova, T. R.; Kurnikov, I. V.; Beratan, D. N. Coupling coherence distinguishes structure sensitivity in protein electron transfer. *Science* **2007**, *315*, 622−625.
(35) Skourtis, S. S.; Beratan, D. N.; Waldeck, D. H. Coherence in electron transfer pathways. *Procedia Chem.* **2011**, *3*, 99−104.
(36) Bao, D.; Millare, B.; Xia, W.; Steyer, B. G.; Gerasimenko, A. A.; Ferreira, A.; Contreras, A.; Vullev, V. I. Electrochemical oxidation of ferrocene: a strong dependence on the concentration of the supporting electrolyte for nonpolar solvents. *J. Phys. Chem. A* **2009**, *113*, 1259−1267.
(37) O'Mari, O.; Vullev, V. I. Electrochemical analysis in charge-transfer science: The devil in the details. *Curr. Opin. Electrochem.* **2022**, *31*, 100862.
(38) Zhu, X.-Y.; Yang, Q.; Muntwiler, M. Charge-transfer excitons at organic semiconductor surfaces and interfaces. *Acc. Chem. Res.* **2009**, *42*, 1779−1787.
(39) Savoie, B. M.; Jackson, N. E.; Chen, L. X.; Marks, T. J.; Ratner, M. A. Mesoscopic features of charge generation in organic semiconductors. *Acc. Chem. Res.* **2014**, *47*, 3385−3394.
(40) Upadhyayula, S.; Bao, D.; Millare, B.; Sylvia, S. S.; Habib, K. M. M.; Ashraf, K.; Ferreira, A.; Bishop, S.; Bonderer, R.; Baqai, S.; Jing, X.; Penchev, M.; Ozkan, M.; Ozkan, C. S.; Lake, R. K.; Vullev, V. I. Permanent Electric Dipole Moments of Carboxyamides in Condensed Media: What Are the Limitations of Theory and Experiment? *J. Phys. Chem. B* **2011**, *115*, 9473−9490.
(41) Zheng, W.; Li, Z.; Chen, K.; Liu, S.; Chi, Z.; Xu, J.; Zhang, Y. Temperature-resistant intrinsic high dielectric constant polyimides: more flexibility of the dipoles, larger permittivity of the materials. *Molecules* **2022**, *27*, 6337.
(42) Krzeszewski, M.; Espinoza, E. M.; Červinka, C.; Derr, J. B.; Clark, J. A.; Borchardt, D.; Beran, G. J.; Gryko, D. T.; Vullev, V. I. Dipole effects on electron transfer are enormous. *Angew. Chem., Int. Ed.* **2018**, *57*, 12365−12369.
(43) Bao, D.; Upadhyayula, S.; Larsen, J. M.; Xia, B.; Georgieva, B.; Nuñez, V.; Espinoza, E. M.; Hartman, J. D.; Wurch, M.; Chang, A.; Lin, C.-K. Dipole-mediated rectification of intramolecular photoinduced charge separation and charge recombination. *J. Am. Chem. Soc.* **2014**, *136* (37), 12966−12973.
(44) Lewis, F. D. Distance Dependent Electronic Interactions Across DNA Base Pairs: Charge Transport, Exciton Coupling, and Energy Transfer. *Isr. J. Chem.* **2013**, *53*, 350−365.
(45) Operamolla, A.; Ragni, R.; Milano, F.; Tangorra, R. R.; Antonucci, A.; Agostiano, A.; Trotta, M.; Farinola, G. "Garnishing" the photosynthetic bacterial reaction center for bioelectronics. *J. Mater. Chem. C* **2015**, *3*, 6471−6478.
(46) Warren, J. J.; Winkler, J. R.; Gray, H. B. Hopping maps for photosynthetic reaction centers. *Coord. Chem. Rev.* **2013**, *257*, 165−170.
(47) Schuster, G. B. Long-range charge transfer in DNA: transient structural distortions control the distance dependence. *Acc. Chem. Res.* **2000**, *33*, 253−260.
(48) Doi, M.; Edwards, S. *The Theory of Polymer Dynamics*; Clarendon: Oxford, 1986; p 317.
(49) Kratky, O.; Porod, G. Röntgenuntersuchung gelöster fadenmoleküle. *Recl. Trav. Chim. Pays-Bas* **1949**, *68*, 1106−1122.
(50) Bustamante, C.; Marko, J. F.; Siggia, E. D.; Smith, S. Entropic elasticity of λ-phage DNA. *Science* **1994**, *265*, 1599−1600.
(51) Hamuro, Y.; Geib, S. J.; Hamilton, A. D. Oligoanthranilamides. Non-peptide subunits that show formation of specific secondary structure. *J. Am. Chem. Soc.* **1996**, *118*, 7529−7541.
(52) Yang, M. Y.; O'Mari, O.; Goddard Iii, W. A.; Vullev, V. I. How Permanent Are the Permanent Macrodipoles of Anthranilamide Bioinspired Molecular Electrets? *J. Am. Chem. Soc.* **2024**, *146*, 5162−5172.
(53) Rappe, A. K.; Goddard Iii, W. A. Charge equilibration for molecular dynamics simulations. *J. Phys. Chem.* **1991**, *95*, 3358−3363.
(54) Van Duin, A. C.; Dasgupta, S.; Lorant, F.; Goddard, W. A. ReaxFF: a reactive force field for hydrocarbons. *J. Phys. Chem. A* **2001**, *105*, 9396−9409.
(55) Naserifar, S.; Brooks, D. J.; Goddard, W. A.; Cvicek, V. Polarizable charge equilibration model for predicting accurate electrostatic interactions in molecules and solids. *J. Chem. Phys.* **2017**, *146* (12), 124117.
(56) Purc, A.; Espinoza, E. M.; Nazir, R.; Romero, J. J.; Skonieczny, K.; Jezewski, A.; Larsen, J. M.; Gryko, D. T.; Vullev, V. I. Gating that suppresses charge recombination−the role of mono-N-arylated diketopyrrolopyrrole. *J. Am. Chem. Soc.* **2016**, *138*, 12826−12832.
(57) Derr, J. B.; Clark, J. A.; Morales, M.; Espinoza, E. M.; Vadhin, S.; Vullev, V. I. Solvent-induced selectivity of Williamson etherification in the pursuit of amides resistant against oxidative degradation. *RSC Adv.* **2020**, *10*, 24419−24424.
(58) Espinoza, E. M.; Larsen-Clinton, J. M.; Krzeszewski, M.; Darabedian, N.; Gryko, D. T.; Vullev, V. I. Bioinspired Approach Toward Molecular Electrets: Synthetic Proteome for Materials. *Pure Appl. Chem.* **2017**, *89*, 1777−1797.
(59) Naserifar, S.; Oppenheim, J. J.; Yang, H.; Zhou, T.; Zybin, S.; Rizk, M.; Goddard, W. A. Accurate non-bonded potentials based on periodic quantum mechanics calculations for use in molecular

https://doi.org/10.1021/acs.jpcb.4c04103
J. Phys. Chem. B 2025, 129, 1750−1759

simulations of materials and systems. *J. Chem. Phys.* **2019**, *151* (15), 154111.
(60) Rappé, A. K.; Casewit, C. J.; Colwell, K.; Goddard Iii, W. A.; Skiff, W. M. UFF, a full periodic table force field for molecular mechanics and molecular dynamics simulations. *J. Am. Chem. Soc.* **1992**, *114*, 10024−10035.
(61) Kuhn, W. Uber die gestalt fadenformiger molekule in losungen. *Kolloid Z* **1934**, *68*, 2−18.
(62) Flory, P. J.; Volkenstein, M. Statistical mechanics of chain molecules. *Biopolymers* **1969**, *8*, 699−700.
(63) Rubinstein, M.; Colby, R. H. *Polymer physics*; Oxford university press, 2003.
(64) Porod, G. Die Röntgenkleinwinkelstreuung von dichtgepackten kolloiden systemen: I. Teil. *Kolloid Z* **1951**, *124*, 83−114.
(65) Hsu, H.-P.; Paul, W.; Binder, K. Standard definitions of persistence length do not describe the local "intrinsic" stiffness of real polymer chains. *Macromolecules* **2010**, *43*, 3094−3102.
(66) Odijk, T. Polyelectrolytes near the rod limit. *J. Polym. Sci. Polym. Phys. Ed.* **1977**, *15*, 477−483.
(67) Skolnick, J.; Fixman, M. Electrostatic persistence length of a wormlike polyelectrolyte. *Macromolecules* **1977**, *10*, 944−948.
(68) Yamakawa, H. *Modern theory of polymer solutions*; Harper & Row, 1971.
(69) Durbin, J.; Watson, G. S. Testing for serial correlation in least squares regression: I. *Biometrika* **1950**, *37*, 409−428.
(70) Durbin, J.; Watson, G. S. Testing for serial correlation in least squares regression. I. In *Breakthroughs in Statistics: methodology and Distribution*; Springer, 1992, pp. 237−259.
(71) Rutledge, D.; Barros, A. Durbin−Watson statistic as a morphological estimator of information content. *Anal. Chim. Acta* **2002**, *454*, 277−295.
(72) Eaton, D. F. Recommended methods for fluorescence decay analysis. *Pure Appl. Chem.* **1990**, *62*, 1631−1648.
(73) Serrano, L.; Fersht, A. R. Capping and α-helix stability. *Nature* **1989**, *342*, 296−299.
(74) Richardson, J. S.; Richardson, D. C. Amino acid preferences for specific locations at the ends of α helices. *Science* **1988**, *240*, 1648−1652.
(75) Sunday, D. F.; Chremos, A.; Martin, T. B.; Chang, A. B.; Burns, A. B.; Grubbs, R. H. Concentration Dependence of the Size and Symmetry of a Bottlebrush Polymer in a Good Solvent. *Macromolecules* **2020**, *53*, 7132−7140.
(76) Baker, E. G.; Bartlett, G. J.; Crump, M. P.; Sessions, R. B.; Linden, N.; Faul, C. F.; Woolfson, D. N. Local and macroscopic electrostatic interactions in single α-helices. *Nat. Chem. Biol.* **2015**, *11*, 221−228.
(77) Presta, L. G.; Rose, G. D. Helix signals in proteins. *Science* **1988**, *240*, 1632−1641.
(78) Shoemaker, K. R.; Kim, P. S.; York, E. J.; Stewart, J. M.; Baldwin, R. L. Tests of the helix dipole model for stabilization of α-helices. *Nature* **1987**, *326*, 563−567.
(79) Lockhart, D. J.; Kim, P. S. Electrostatic screening of charge and dipole interactions with the helix backbone. *Science* **1993**, *260*, 198−202.
(80) Sengupta, D.; Behera, R. N.; Smith, J. C.; Ullmann, G. M. The α helix dipole: screened out? *Struct.* **2005**, *13*, 849−855.
(81) Fairman, R.; Shoemaker, K. R.; York, E. J.; Stewart, J. M.; Baldwin, R. L. Further studies of the helix dipole model: Effects of a free αNH3+ or α-COO− group on helix stability. *Prot. Struct. Funct. Bioinf.* **1989**, *5*, 1−7.
(82) Aurora, R.; Rosee, G. D. Helix capping. *Protein Sci.* **1998**, *7*, 21−38.
(83) Beratan, D. N.; Liu, C.; Migliore, A.; Polizzi, N. F.; Skourtis, S. S.; Zhang, P.; Zhang, Y. Charge transfer in dynamical biosystems, or the treachery of (static) images. *Acc. Chem. Res.* **2015**, *48*, 474−481.
(84) Robertson, N.; McGowan, C. A. A comparison of potential molecular wires as components for molecular electronics. *Chem. Soc. Rev.* **2003**, *32*, 96−103.
(85) Gilbert, M.; Albinsson, B. Photoinduced charge and energy transfer in molecular wires. *Chem. Soc. Rev.* **2015**, *44*, 845−862.
(86) Schubert, C.; Margraf, J.; Clark, T.; Guldi, D. Molecular wires−impact of π-conjugation and implementation of molecular bottlenecks. *Chem. Soc. Rev.* **2015**, *44*, 988−998.
(87) Marin-Gonzalez, A.; Vilhena, J.; Perez, R.; Moreno-Herrero, F. A molecular view of DNA flexibility. *Q. Rev. Biophys.* **2021**, *54*, No. e8.
(88) Ouldridge, T. E.; Louis, A. A.; Doye, J. P. Structural, mechanical, and thermodynamic properties of a coarse-grained DNA model. *J. Chem. Phys.* **2011**, *134*, 085101.
(89) Ratajczyk, E. J.; Šulc, P.; Turberfield, A. J.; Doye, J. P.; Louis, A. A. Coarse-grained modeling of DNA−RNA hybrids. *J. Chem. Phys.* **2024**, *160*, 115101.
(90) Guilbaud, S.; Salomé, L.; Destainville, N.; Manghi, M.; Tardin, C. Dependence of DNA persistence length on ionic strength and ion type. *Phys. Rev. Lett.* **2019**, *122*, 028102.
(91) Hatcher, E.; Balaeff, A.; Keinan, S.; Venkatramani, R.; Beratan, D. N. PNA versus DNA: effects of structural fluctuations on electronic structure and hole-transport mechanisms. *J. Am. Chem. Soc.* **2008**, *130*, 11752−11761.
(92) Chhetri, K. B.; Sharma, A.; Naskar, S.; Maiti, P. K. Nanoscale structures and mechanics of peptide nucleic acids. *Nanoscale* **2022**, *14*, 6620−6635.
(93) Sontz, P. A.; Muren, N. B.; Barton, J. K. DNA charge transport for sensing and signaling. *Acc. Chem. Res.* **2012**, *45*, 1792−1800.
(94) Wilcox, K. G.; Dingle, M. E.; Saha, A.; Hore, M. J.; Morozova, S. Persistence length of α-helical poly-l-lysine. *Soft Matter* **2022**, *18*, 6550−6560.
(95) Garbuio, L.; Lewandowski, B.; Wilhelm, P.; Ziegler, L.; Yulikov, M.; Wennemers, H.; Jeschke, G. Shape persistence of polyproline II helical oligoprolines. *Chem.—Eur. J.* **2015**, *21*, 10747−10753.
(96) Sahoo, H.; Roccatano, D.; Hennig, A.; Nau, W. M. A 10-Å Spectroscopic Ruler Applied To Short Polyprolines. *J. Am. Chem. Soc.* **2007**, *129*, 9762−9772.
(97) Le Bailly, B. A.; Byrne, L.; Diemer, V.; Foroozandeh, M.; Morris, G. A.; Clayden, J. Flaws in foldamers: conformational uniformity and signal decay in achiral helical peptide oligomers. *Chem. Sci.* **2015**, *6*, 2313−2322.
(98) O'Donnell, J. F.; Mann, C. K. Controlled-potential oxidation of aliphatic amides. *J. Electroanal. Chem. Interfacial Electrochem.* **1967**, *13*, 157−162.
(99) Cordes, M.; Köttgen, A.; Jasper, C.; Jacques, O.; Boudebous, H.; Giese, B. Influence of amino acid side chains on long distance electron transfer in peptides: electron hopping via "stepping stones. *Angew. Chem., Int. Ed.* **2008**, *47*, 3461−3463.
(100) Shlizerman, C.; Atanassov, A.; Berkovich, I.; Ashkenasy, G.; Ashkenasy, N. De novo designed coiled-coil proteins with variable conformations as components of molecular electronic devices. *J. Am. Chem. Soc.* **2010**, *132*, 5070−5076.

NOTE ADDED AFTER ASAP PUBLICATION

This paper was published November 20, 2024, with an error in equation 3b. The corrected version reposted January 9, 2025.

https://doi.org/10.1021/acs.jpcb.4c04103
J. Phys. Chem. B 2025, 129, 1750−1759